Vascular Endothelial Cells Minimize the Total Force on Their Nuclei

A. L. Hazel and T. J. Pedley
Department of Applied Mathematics and Theoretical Physics, University of Cambridge, Silver Street, Cambridge, CB3 9EW, United Kingdom

ABSTRACT The vascular endothelium is a cellular monolayer that lines the arterial walls. It plays a vital role in the initiation and development of atherosclerosis, an occlusive arterial disease responsible for 50% of deaths in the Western world. The focal nature of the disease suggests that hemodynamic forces are an important factor in its pathogenesis. This has led to the investigation of the effects of mechanical forces on the endothelial cells themselves. It has been found that endothelial cells do respond to stresses induced by the flowing blood; in particular, they elongate and align with an imposed flow direction. In this paper, we calculate the distribution of force exerted on a three-dimensional hump, representing the raised cell nucleus, by a uniform shear flow. It is found that, for a nonaxisymmetric ellipsoidal hump, the least total force is experienced when the hump is aligned with the flow. Furthermore, for a hump of fixed volume, there is a specific aspect ratio combination that results in the least total force upon the hump, (0.38 : 2.2 : 1.0; height : length : width). This is approximately the same as the average aspect ratio taken up by the cell nuclei in vivo (0.27 : 2.23 : 1.0). It is possible, therefore, that the cells respond to the flow in such a way as to minimize the total force on their nuclei.

INTRODUCTION

The understanding and hence treatment of atherosclerosis is one of the major goals of current medical research. The vascular endothelium is now understood to be crucial in the pathogenesis of the disease (Ross, 1993). The effects of the fluid mechanical forces, which act on the vascular endothelium, on the development of the disease were initially investigated almost thirty years ago. Abnormally high shear rates can cause endothelial damage (Fry, 1968), whereas the location of atherosclerotic plaques is correlated with regions of low and oscillatory shear (Caro et al., 1971; Ku et al., 1985).

Further studies demonstrated that there were morphological differences between endothelial cell nuclei at different locations around the circulatory system (Flaherty et al., 1972). In the large arteries, the nuclei are elliptical in shape and their longest (or major) axes align with the direction of flow. If the direction of flow is changed, the nuclei will reorient themselves to remain aligned with the flow. In regions of weaker hemodynamic forces, the nuclei are more rounded and have no preferred direction. Subsequent in vitro experiments have demonstrated that uniform, laminar shear causes entire cells grown in static culture to elongate and align with the imposed flow direction (Dewey et al., 1981), together with a rearrangement of the actin cytoskeleton (Herman et al., 1987). Conversely, in a disturbed flow, there is no observed alignment, but cell turnover is increased (Davies et al., 1986). This increased cell turnover renders the endothelium more permeable to large molecules, leading to the cell turnover–leaky junction hypothesis (Weinbaum et al., 1985). The precise nature of the force transmission and transduction across the cell is still unknown; although it is believed to depend upon tyrosine kinase activity, intracellular calcium, and an intact microtubule network (Davies, 1995; Malek and Izumo, 1996). Friedman and Fry (1993) developed a model in which the local permeability of the endothelium is altered during the adaptive response to wall shear stress. This model has subsequently shown reasonable agreement with experimental data (Henderson et al., 1994), suggesting that the details of the adaptive response may be crucial in the pathogenesis of atherosclerosis.

A theoretical model of the endothelium as a sinusoidal wavy surface has demonstrated that, as might be expected, the uneven endothelial surface leads to a nonuniform shear stress distribution at the cellular level (Satcher et al., 1992). The shear stress distribution was calculated by solving the Stokes equations using a linear approximation to the wavy surface when its displacement was small, and a numerical method for larger surface displacements. The perturbation shear stress due to the wavy surface was found to be as large as 34% in some cases, with the peak wall shear stresses at the crests of the wavy surface. The surface geometry corresponding to an aligned monolayer, however, was subject to reduced forces and shear stress gradients, compared to nonaligned geometries.

The use of atomic force microscopy has recently allowed measurement of the endothelial surface topography in vitro for the first time (Barbee et al., 1994). It was found that the unsheared cells had an aspect ratio (length/width) of 1.12 ± 0.31 and a height of 3.39 ± 0.70 μm, whereas, after exposure to a uniform shear flow, these became 2.16 ± 0.53 and 1.77 ± 0.52 μm. It has now been confirmed that the

Received for publication 29 March, 1999 and in final form 8 October 1999.

Address reprint requests to Andrew L. Hazel, Biomedical Engineering Center, Ohio State University, 270 Bevis Hall, 1080 Carmack Road, Columbus, OH 43210. Tel.: 614-688-5447; Fax: 614-292-7301; E-mail: andrew@chopin.bme.ohio-state.edu.

Dr. Hazel's present address is Biomedical Engineering Center, Ohio State University, 270 Bevis Hall, 1080 Carmack Road, Columbus, OH 43210.

0006-3495/00/01/47/08 $2.00

aspect ratios and heights for endothelial cells in situ are very similar to those in vitro (Davies et al., 1995). Barbee et al. (1995) used the measured endothelial surface as a boundary condition in the numerical solution of the Stokes equations. The results showed that the alignment of the cells resulted in lower average peak wall shear stresses and shear stress gradients per cell. The relative areas exposed to extremes of shear stress and shear stress gradient were also reduced in the aligned geometries.

Yamaguchi and Yamamoto (1995) have studied the effects of wall shear stress on the alignment of endothelial cells using computational fluid dynamics. The shape of the endothelial cells was modeled using a two-dimensional (2D) Gaussian distribution, and the cells were initially distributed with their long axis at a random angle to the direction of the oncoming flow. The wall shear stress at the top of the cells was calculated and then the angles of orientation were adjusted by a fixed amount in a random direction. The wall shear stress was recalculated and, if it was found to be higher at the new orientation, then the cell orientation was reset to its previous value. After a long time, it was found that the cells had all aligned in the direction of the flow, indicating that this configuration does indeed lead to the lowest peak wall shear stress. Yamamoto and Yamaguchi (1997) further refined this study by allowing the model cells to deform as well as rotate, again recomputing the wall shear stress at the top of the cell after each morphologic change. The volume of the cells was assumed to be fixed and, after a long time, the cells were again found to have aligned with the flow and also to have elongated in a manner similar to that observed in in vitro experiments.

In this paper, the flow over a somewhat idealized cell, consisting of a single nucleus, raised above the cellular monolayer, is initially considered. The nuclei of endothelial cells do protrude above the rest of the cellular surface, but this surface is not perfectly flat, as assumed here. The hope is that this model will provide a valuable insight into the forces experienced by each cell and the mechanisms whereby it is reduced. It is argued below that the effects of additional nuclei upon the forces on an individual nucleus are expected to be negligible.

The volume of the nucleus, projecting above the rest of the cell membrane, is assumed to be constant, but this is not necessarily the case in vivo. There are, of course, physical limitations on the nuclear shape, because it cannot become infinitely thin, but this does not ensure constant volume. The measurements of Chung and Min (1998) have demonstrated, however, that the endothelial cells retain a fixed volume throughout the morphologic changes induced by fluid flow in vitro. The volumes computed were based upon microscopically visualized endothelial surfaces, rather than entire cells, with the bulk of the volume corresponding to the nuclear volume projecting above the rest of the cell.

MODELING ASSUMPTIONS AND METHODS

In the large arteries, the height of the endothelium, $\mathcal{O}(\mu\text{m})$, is very much smaller than the arterial diameter, $\mathcal{O}(\text{mm})$, and the heart rate is typically about 1–2 Hz, with the consequence that the local fluid behavior is quasisteady and is dominated by viscous forces. Moreover, the wall curvature may be neglected. A further consequence is that, on the length scale of the cell, the oncoming velocity profile will be a quasisteady linear shear.

The blood is modeled as an incompressible, homogeneous, Newtonian fluid. The homogeneity must be questioned, because, on the cellular length scale, the presence of red blood cells and other particles should not be ignored. The existence of a thin cell-free zone (plasma layer) at the edges of the blood vessels (Fåhræus, 1929) implies that the red blood cells will not be concentrated close to the wall, however, and this may in part justify neglecting interactions between the endothelial cells and the red blood cells. The Newtonian assumption is a simplification, but it is not unreasonable, because the plasma, which will compose the bulk of the fluid near the wall, is known to be well approximated by a Newtonian model (Pedley, 1980).

The other major simplification in this model is the neglect of the endothelial cell glycocalyx, which is a thin layer, between 50 and 80 nm in the arteries and up to 1 μm in the capillaries (Wang and Parker, 1995), of extracellular membrane glycoproteins adsorbed onto the surface of the cell. The glycocalyx has been previously modeled as a biphasic mixture, or porous layer, with a linearly elastic solid phase and a Newtonian viscous fluid phase (Wang and Parker, 1995; Damiano et al., 1996). These models indicate that the glycocalyx can act as a "force buffer," leading to lower fluid wall shear stresses and wall shear stress gradients at the endothelial surface than in the absence of the layer; a consequence of the flow being restricted in the porous layer.

We consider a uniform shear flow of incompressible, Newtonian fluid encountering an arbitrary three-dimensional (3D) hump, which represents the raised cell nucleus, on an infinite flat plate, see Fig. 1. The problem is posed in Cartesian coordinates, where the $\hat{x}$- and $\hat{y}$-axes are in the plane of the wall, $\hat{z} = 0$, and the $\hat{z}$-axis is the normal.

The reference length scale of the hump is $\hat{\mathcal{R}} = \delta\hat{a}$, where $\hat{a}$ is the diameter of the tube and $\delta \ll 1$; the length, $\hat{l}$, height, $\hat{h}$, and width, $\hat{w}$, of the hump are all assumed to be $\mathcal{O}(\hat{\mathcal{R}})$. We further assume that there is an oncoming Poiseuille flow in the tube, but, at the length scale of the hump, any flow will approximate to a linear shear flow so that $\hat{u} = \hat{S}\hat{z}$, the velocity being in the $\hat{x}$-direction; $\hat{v}$ is the velocity in the $\hat{y}$-direction, and $\hat{w}$ is that in the $\hat{z}$-direction. We define the main flow Reynolds number, Re, to be $\mathrm{Re} = \hat{S}\hat{a}^2/\hat{\nu}$, where $\hat{\nu}$ is the kinematic viscosity of the fluid, and suppose that it is much greater than one. On the length scale of the hump, the Reynolds number is $\mathrm{Re}_h = \hat{S}\hat{\mathcal{R}}^2/\hat{\nu} = \delta^2\mathrm{Re}$ which is

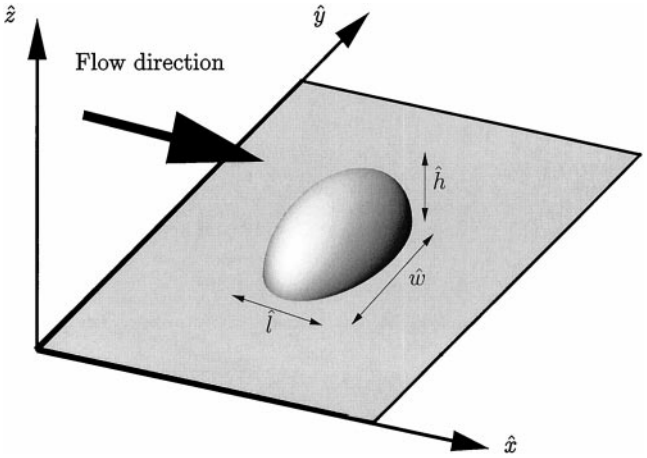

FIGURE 1 Schematic of the problem.

taken to be much less than one. A hat denotes a dimensional quantity and we nondimensionalize by letting:

$$\hat{u} = \hat{S}\hat{a}[\delta u^{P} + U(\delta z)], \tag{1a}$$

$$\hat{v} = \hat{S}\hat{a}\delta v^{P}, \tag{1b}$$

$$\hat{w} = \hat{S}\hat{a}\delta w^{P}, \tag{1c}$$

$$\hat{p} = \hat{\rho}\hat{S}^{2}\hat{a}^{2}\mathrm{Re}^{-1}p, \tag{1d}$$

$$\hat{\mathbf{x}} = \delta\hat{a}\mathbf{x}, \tag{1e}$$

where $\hat{\rho}$ is the density of the fluid, $U(\xi) = \xi + \mathbb{O}(\xi^2)$ is the nondimensional basic Poiseuille flow in the parent tube, p is the dimensionless pressure and $\mathbf{u}^{P}$ is the dimensionless perturbation velocity field induced by the hump.

On substitution of Eqs. 1a–1e into the Navier–Stokes equations and, neglecting the terms of $\mathbb{O}(\delta^2\mathrm{Re})$, we obtain the Stokes equations,

$$\nabla^2\mathbf{u}^{P} = \nabla p, \tag{2}$$

together with the equation of continuity

$$\nabla\cdot\mathbf{u}^{P} = \mathbf{0}, \tag{3}$$

because we are assuming that the fluid is incompressible.

The boundary conditions are that of no-slip on the rigid boundary,

$$u^{P} = -\lambda H(x, y), \quad v^{P} = 0, \quad w^{P} = 0, \quad \text{on } z = \lambda H(x, y), \quad \text{(on hump)}, \tag{4a}$$

$$\mathbf{u}^{P} = \mathbf{0}, \quad \text{on } z = 0, \quad \text{(not on hump)},$$

where $H(x, y)$ is an $\mathbb{O}(1)$ function describing the shape of the hump, $\lambda = \hat{h}/\hat{\mathcal{R}}$ is the scaled height of the hump; and also that the perturbation to the main flow tends to zero as $z \to \infty$

$$\mathbf{u}^{P} \to \mathbf{0}, \quad \text{as } z \to \infty. \tag{4b}$$

This model has been formulated to apply in the large arteries, i.e., diameters of $\mathbb{O}$(mm), in which atherosclerosis tends to develop. The local fluid mechanical behavior near endothelial cells is always dominated by viscous forces, however, owing to the relatively small dimensions involved. Gaver and Kute (1998) found that, in 2D channel flow, the opposite wall does not affect the shear stresses on an obstacle until the obstacle occupies more than 25% of the channel width. Furthermore, they found good agreement between their 2D calculations and previous 3D results, when the gap width between the top of the cell and the opposite wall was small. This suggests that the present model is also applicable to the majority of in vitro experiments, in which the endothelium is subjected to a linear shear flow by means of a parallel plate or cone-and-plate device. The gap width in these experiments is usually much greater than four times the height of the cellular monolayer. The model is not directly applicable to flow in smaller arteries, arterioles, and capillaries, because the neglected wall curvature effects will become important there, but the qualitative results are expected to remain unchanged.

The study of creeping flow over an obstacle or cavity surrounded by a plane wall is not a new one and it has many applications. Important examples are: displacement of fluid droplets from solid surfaces (Dussan, 1987; Brooks and Tozeren, 1996; Li and Pozrikidis, 1996; Dimitrakopoulos and Higdon, 1997), which find applications in industrial drying processes and biological problems of cell adhesion (Basmadjian, 1984; Olivier and Truskey, 1993; Gaver and Kute, 1998); and also problems in erosion, corrosion, and etching processes (Alkire et al., 1990; Shin and Economou, 1991).

It is convenient to formulate the problem as an integral equation,

$$\mathbf{u}^{P}(\mathbf{x}) = -\int_{\mathcal{H}} \mathbf{f}(\mathbf{x}_0)\cdot\mathbf{G}^{W}(\mathbf{x}_0, \mathbf{x})\, dS(\mathbf{x}_0), \tag{5}$$

where $\mathcal{H}$ is the surface of the hump, $\mathbf{f}$ is the surface traction on the hump and $\mathbf{G}^{W}$ is the Green's function tensor due to a plane wall,

$$G^{W}_{ij}(\mathbf{x}_0, \mathbf{x}) = \mathcal{G}_{ij}(\mathbf{x}_0, \mathbf{x}) - \mathcal{G}_{ij}(\mathbf{x}_0, \mathbf{x}^{I}) + 2z^2 G^{D}_{ij}(\mathbf{x}_0, \mathbf{x}^{I}) - 2z G^{SD}_{ij}(\mathbf{x}_0, \mathbf{x}^{I}), \tag{6}$$

where, $\mathbf{x}^{I} = (x, y, -z)$, the image of $\mathbf{x}$ with respect to the wall, and

$$\mathcal{G}_{ij}(\mathbf{x}_0, \mathbf{x}) = \frac{1}{8\pi}\left(\frac{\delta_{ij}}{|\mathbf{x}_0 - \mathbf{x}|} + \frac{(\mathbf{x}_0 - \mathbf{x})_i(\mathbf{x}_0 - \mathbf{x})_j}{|\mathbf{x}_0 - \mathbf{x}|^3}\right), \tag{7a}$$

$$G^{D}_{ij}(\mathbf{x}_0, \mathbf{x}) = \pm^{1,2}_{3}\frac{1}{8\pi}\left(\frac{\delta_{ij}}{|\mathbf{x}_0 - \mathbf{x}|^3} - 3\frac{(\mathbf{x}_0 - \mathbf{x})_i(\mathbf{x}_0 - \mathbf{x})_j}{|\mathbf{x}_0 - \mathbf{x}|^5}\right), \tag{7b}$$

$$G_{ij}^{SD}(\mathbf{x}_0, \mathbf{x}) = (\mathbf{x}_0 - \mathbf{x})_3 G_{ij}^{D}(\mathbf{x}_0, \mathbf{x}) \pm_3^{1,2} \frac{1}{8\pi} \frac{\delta_{j3}(\mathbf{x}_0 - \mathbf{x})_i - \delta_{i3}(\mathbf{x}_0 - \mathbf{x})_j}{|\mathbf{x}_0 - \mathbf{x}|^3}, \quad (7c)$$

where the $\pm_3^{1,2}$ means there is a minus sign for $j = 3$, the z-direction, and a plus sign for $j = 1, 2$, the x- and y-directions.

$G^W(\mathbf{x}_0, \mathbf{x}) \cdot \mathbf{g}$ is defined to be the velocity field due to a point source of strength $\mathbf{g}$ placed at $\mathbf{x}_0$, with the additional constraint that the velocity is zero on the plane $z = 0$. This constraint restricts the domain of integration in Eq. 5 to the surface of the hump. The physical interpretation of Eq. 5 is that the hump surface is approximated by a collection of point forces of different strengths; the total velocity field is then the sum of the velocity fields due to all the point forces. A complete derivation of Eq. 5 from the Stokes equations can be found in Pozrikidis (1992).

The no-slip condition, Eq. 4a, implies that the value of $\mathbf{u}^P$ is known on the surface of the hump. This leads to a Fredholm integral equation of the first kind for the surface traction $\mathbf{f}$, which is solved numerically using a boundary element collocation method (Pozrikidis, 1992; Banerjee, 1994). The code was validated by comparing the computed forces and torques with the analytic solutions for a hemisphere (Price, 1985) and sphere in point contact with the wall (O'Neill, 1968) and also computations for axisymmetric spherical caps and spheroids (Pozrikidis, 1997).

Table 1 shows the nondimensional total force parallel to the plane $z = 0$ on spherical caps of semiangle α. The first column shows the results of the axisymmetric computations of Pozrikidis, in which 32 line elements were used. These results are accurate to three significant figures. The second column shows the results from the 3D boundary element code using only 20 quadratic surface elements, or 24 in the case $\alpha = 1.0$. The results are accurate to within a reasonably small percentage error, giving confidence in the results. If 165 elements are used, then the results are accurate to the three significant figures given by Pozrikidis; however, this dramatically increases the cost of the procedure.

TABLE 1 Comparison of nondimensional force on spherical caps for axisymmetric and 3D boundary element methods

α	Axisymmetric	3D	Percentage Error
1.0	10.2*	10.2	0.0
0.9	9.92	9.85	0.7
0.8	9.07	8.97	1.1
0.7	7.73	7.61	1.6
0.6	6.06	5.94	2.0
0.5	4.30*	4.21	2.1
0.4	2.69	2.64	1.9
0.3	1.41	1.38	2.1
0.2	0.555	0.545	1.8
0.1	0.118	0.114	3.4

*These results correspond to the analytical results given by O'Neill (1968) and Price (1985), which are 10.205 and 4.30, respectively.

The numerical model is very flexible and can be used to determine the key features of Stokes flow about an arbitrary 3D body, having at least one point of contact with a plane wall. In this paper, we consider the effects of varying the shape and angle to the flow of the hump upon the total force experienced.

The linearity of the governing Eq. 5 implies that the solution for a linear shear flow at an arbitrary angle θ to the x-axis is $\mathbf{f} = \mathbf{f}_x \cos\theta + \mathbf{f}_y \sin\theta$, where $\mathbf{f}_x$ is the force when the flow is in the x-direction ($\theta = 0$) and $\mathbf{f}_y$ is the force due to a flow in the y-direction ($\theta = \pi/2$). Thus, the force distribution, and hence the velocity field for the general case, can be reconstructed from just two simple cases.

In all cases considered here, the obstacle is restricted to that of a semiellipsoid, in accordance with experimental observations of the elliptical nature of endothelial cell nuclei in vivo (Flaherty et al., 1972). The theoretical model of the endothelial cell as a membrane stretched over a spherical nucleus (Fung and Liu, 1993) gives a shape that falls off in a more realistic Gaussian manner away from the nucleus. The extra Gaussian tails are not expected to have a large effect on the total force, however. There are three geometric parameters that govern the problem: λ_l, the length-to-width ratio, and λ_h, the height-to-width ratio, together with the volume of the ellipsoid. The total force on the hump is found by integrating the force vectors over the surface of the hump,

$$\mathbf{F} = \int_{\mathcal{H}} \mathbf{f}(\mathbf{x}_0)\, dS(\mathbf{x}_0).$$

If the axes of the ellipsoid in the plane $z = 0$ are chosen to lie along the x and y axes, then the inherent symmetries imply that $\mathbf{F}_x = (\mathcal{F}_x, 0, 0)$ and $\mathbf{F}_y = (0, \mathcal{F}_y, 0)$. It follows that $\mathbf{F} = (\mathcal{F}_x \cos\theta, \mathcal{F}_y \sin\theta, 0)$ and, hence, the magnitude of the total force on the hump is

$$|\mathbf{F}| = \sqrt{\mathcal{F}_x^2 \cos^2\theta + \mathcal{F}_y^2 \sin^2\theta}.$$

Elementary calculus shows that the extrema of $|\mathbf{F}|$ occur when $\theta = 0$ or $\pi/2$, so that

$$|\mathbf{F}|_{max} = \max\{\mathcal{F}_x, \mathcal{F}_y\} \quad \text{and} \quad |\mathbf{F}|_{min} = \min\{\mathcal{F}_x, \mathcal{F}_y\}.$$

In other words, the minimum total force on the hump, for a shear flow at an arbitrary angle is the minimum of the two cases $\theta = 0$ (flow in x-direction) and $\theta = \pi/2$ (flow in y-direction). Equivalently, it is the minimum of the two extreme cases when the semimajor axis of the ellipsoid in the plane $z = 0$ is aligned with the flow or perpendicular to it.

RESULTS

Numerical studies were performed to determine the values of $\mathcal{F}_x$ and $\mathcal{F}_y$ for a variety of geometric parameters. It was

found that the maximum total force is experienced when the major axis of the ellipsoid is perpendicular to the flow and the minimum when it is aligned. Thus, for any nonaxisymmetric semiellipsoid, the minimum force occurs when the major axis is aligned with the flow.

Figure 2 shows contours of the total nondimensional force, $|\mathbf{F}|$, on an aligned hump with a fixed volume plotted against the aspect ratios λ_h and λ_l.

The dimensional force is $\pi\hat{\mu}\hat{S}\hat{\mathcal{R}}^2|\mathbf{F}|$, where $\hat{\mu}$ is the viscosity of the fluid, $\hat{S}$ is the shear rate and $\hat{\mathcal{R}}$ is the reference length scale (see Modeling Assumptions and Methods), which is chosen to be the radius of the hemisphere with the same volume as the hump. In this case, the flow is always in the *x*-direction, the length is in the *x*-direction, width in the *y*-direction, and height in the *z*-direction (see Fig. 1). Thus, if $\lambda_l > 1.0$, the cell is aligned with the flow, whereas, if $\lambda_l < 1.0$, the cell is perpendicular to the flow. If $\lambda_l = 1.0$, the cell is axisymmetric about the *z*-axis. Note that, in the case of the hemisphere ($\lambda_l = 1.0$, $\lambda_h = 0.5$), the nondimensional force is 4.30, agreeing with the previous results of Price (1985).

For a fixed λ_l and a sufficiently large λ_h, there is a drop in total force, with decreasing λ_h, which is due to the corresponding drop in height of the hump. This trend continues until the drop in peak traction is balanced by the increase in surface area owing to the fixed volume constraint. When λ_h is very small, the surface area must be large and hence the total force is large, despite the fact that the peak traction will be small.

For a fixed λ_h and a sufficiently small λ_l, there is a drop in total force with increasing λ_l, because the hump becomes more and more elongated in the flow direction; effectively, the width of the hump is decreasing. Once again, there is a minimum point, after which the decrease in peak traction can no longer be balanced by the increasing surface area.

There is an overall minimum of the total force at $\lambda_l \approx 2.2$ and $\lambda_h \approx 0.38$. This compares very well with the average aspect ratio of the cell nuclei throughout the circulatory system, which is $\lambda_l = 2.23$, where the width is 6.6 μm and the length is 14.8 μm (Flaherty et al., 1972). The recent atomic force microscopy data indicates that, in shear flow conditions both in vitro and in situ, the height of the cell nucleus is approximately 1.77 μm (Barbee et al., 1994), corresponding to $\lambda_h = 0.27$. Thus, the estimated average aspect ratios of the nuclei in vivo are very close to the theoretical minimum force configuration.

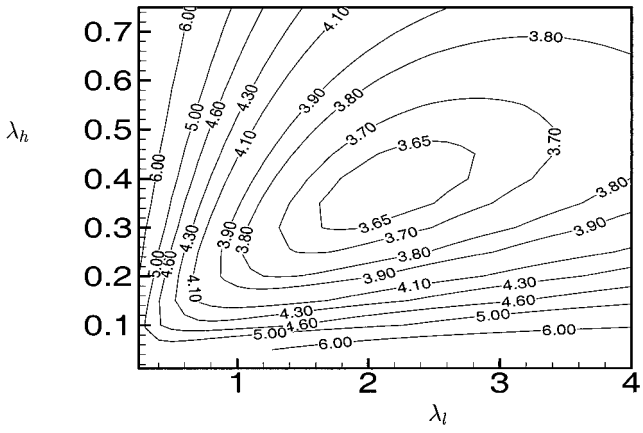

FIGURE 2 Contours of total force on an aligned hump of fixed volume in λ_l–λ_h parameter space.

DISCUSSION

The results indicate that, for any semiellipsoidal hump in a shear flow, the least total force is experienced when the longest axis is aligned with the flow direction. This configuration minimizes the width of the obstacle encountered by the fluid and, therefore, minimizes the pressure force on the hump, which is related to its frontal area. Consequently, there will be lower peak tractions and hence a lower total force on the obstacle. The nature of this mechanism suggests that the same result will hold for a general obstacle. That is, the least total force will be experienced when the smallest overall width is perpendicular to the flow. The experimental results of Flaherty et al. (1972) and Dewey et al. (1981) indicate that the cells do indeed orient themselves in this manner. Note also that, if the nuclear shape is a direct consequence of hemodynamic forces, the reversibility of Stokes flow implies a fore–aft symmetry, as observed.

For a hump of fixed volume, decreasing λ_h results in a decrease in peak traction. This is due to two effects. First, the viscous stresses in a linear shear flow increase with height, and, so, reducing the height of the hump will result in a lower shear force on it. The area of the hump perpendicular to the flow is also reduced, which will result in a lower viscous pressure force. Increasing λ_l leads to a decrease in peak traction, which is due purely to the reduction in width of the obstacle and the consequent reduction in pressure force.

It was also found that, for a fixed volume of hump, there is a specific aspect ratio combination that results in the lowest total force experienced. This minimum arises as a balance between the lowering of the peak tractions, as the height and width of the hump are reduced, and the accompanying increase in surface area due to the fixed volume constraint. The calculated minimum agrees very well with the average aspect ratio taken up by endothelial cell nuclei in vivo. The minimum is very broad, however, and therefore small changes in aspect ratio will not have a great effect on the total force. In fact, the range of nuclear aspect ratios, λ_l, observed by Flaherty et al. (1972) is 1.39 to 2.91, which, for realistic values of λ_h, is enclosed within the contour line representing a nondimensional total force of 3.80. The deviation from the minimum total force value is less than 5% over this entire range of aspect ratios.

This relative insensitivity of force to shape has also been observed by Basmadjian (1984) and Olivier and Truskey (1993). Basmadjian (1984) collected results, both theoretical and experimental, on the forces experienced by various obstacles on plane walls. It was found that, in the case of small protrusions, the drag coefficients were similar for quite different geometries. Olivier and Truskey (1993) calculated the forces and torques on four different 2D endothelial cell shapes, representing stages of cell spreading during adhesion to a flat plate. They found that the drag force varies little with cell shape and was only reduced by a factor of two in the rather extreme transition from initial attachment to a fully spread cell.

There are several simplifications in this model. First, the endothelial cell nuclei are not isolated in vivo and exist in confluent monolayers. The linearity of Stokes flow allows the case of several nuclei in a monolayer to be constructed by addition of the velocity fields for isolated nuclei in different locations. The force on each hump will be that due to itself, plus contributions from the velocity fields due to the surrounding humps. The typical internuclear spacing is $\mathcal{O}(10\ \mu\text{m})$, several times the typical nuclear dimensions, which are $\mathcal{O}(1\ \mu\text{m})$. Expansion of the Green's function indicates that the velocity field decays as $\mathcal{O}(1/r^2)$, as the distance, r, from the hump increases. This results in decay of the perturbation pressure and shear stress as $\mathcal{O}(1/r^3)$. Thus, the contribution to the force on the nucleus from other nuclei will be approximately 1000 times smaller than the force due to itself, and the force on a cell nucleus in a confluent monolayer will be approximately that experienced by a single nucleus. This result will hold only if Stokes flow is a valid approximation throughout the monolayer, however. At a distance far enough away from the cell nucleus, the Stokes equations break down, and weak inertial effects become important. Estimates suggest that this distance is $\mathcal{O}(50\ \mu\text{m})$, a cellular, rather than a nuclear, length scale. The presence of such inertial effects may explain why the endothelial cells are not of a uniform shape even in in vitro experiments, where the macroscopic flow conditions are uniform (Levesque and Nerem, 1985; Davies et al., 1995). The Stokes flow calculation would suggest that, if the cells are aiming to minimize the total force on their nuclei, they would all adopt the same shape, and this is not the case. Thus, although the average total force on an endothelial cell nucleus will be approximated well by the Stokes flow solution, the individual cell-to-cell variability may be a consequence of inertia, which will certainly affect the local distribution of wall shear stress.

The assumption of a fixed volume is also to be viewed critically. The assumption corresponds to the volume of the nucleus that projects above the rest of the cell being constant, and the good agreement between the theory and the in vivo measurements indicates that this may be the case, assuming that the cells are aiming to experience the minimum total force. The lack of change in this volume may be a consequence of the cell volume regulatory mechanisms. These mechanisms control the volume of the entire cell, rather than that of the nuclear bulge protruding above it, but may still be of some relevance. There are several such volume-regulatory mechanisms in cells, because a major change in volume will damage the integrity of the cell (see the review given by Lang et al., 1998). The regulatory cell-volume increase and decrease is mainly accomplished by the transport of ions, particularly potassium and sodium, across the cell membrane, altering the osmotic potential of the cell, and hence the volume, within minutes. A large ion imbalance will interfere with numerous cell functions, and so, cells also produce osmolytes, molecules that change the osmotic potential without compromising other cell functions even at high concentrations. The accumulation of these molecules is a much slower process than ionic transport, taking hours or days. The ionic transfer mechanism will certainly be active over the time scales taken for the morphologic change and would be expected, therefore, to keep the cell volume approximately constant.

The presence of a glycocalyx has been shown to lead to reduced forces on the endothelial surface in theoretical models of flow in capillaries (Damiano et al., 1996). The flow is restricted through the glycocalyx, which is often modeled as a porous layer, and this leads to the lower fluid stresses. The aspect ratio leading to the minimum total force is, however, a relative result and, although the presence of a glycocalyx will undoubtedly alter the actual values of the forces on the nucleus, the location of the minimum is unlikely to change.

It is also interesting to note that the nuclear shape leading to the minimum total force is independent of the magnitude of the shear stress, something that is certainly not true of the endothelial cell alignment observed in vitro (Dewey et al., 1981). At low values of wall shear stresses, the cells do not exhibit any morphologic changes. The mechanical force-detection mechanism of the cell, which is likely to involve strains induced in the cytoskeleton, will almost certainly have a threshold level and is not activated at low wall shear stresses. It is also possible that this threshold is due to other elements in the cell, which respond to the signals emitted by the primary wall shear stress transduction mechanism. As the wall shear stress increases, the cells are observed to elongate further (Levesque and Nerem, 1985). This may be a consequence of an impairment of the volume regulatory mechanism. It is also possible that the cells will not tolerate a shear stress above a certain level anywhere on the cell surface. To reduce the peak wall shear stress, the height must be reduced, leading to further elongation, assuming the volume constraint is valid. It should also be noted that the results of Levesque and Nerem (1985) concern the entire cell shape, not the nuclear behavior, and that the shape of the nucleus may remain unaltered, while the cells themselves continue to elongate.

There are, of course, several other factors that will affect the forces experienced by the cells. The cells are tethered to a basement substrate and will experience forces at this location, as well as at the surface exposed to the blood. The precise response of the cells to mechanical forces will depend upon the internal distribution of these forces; a distribution determined by the structural and mechanical properties of the cells. These properties are still incompletely understood, although progress has been made via the models of Ingber (1998) and Fung and Liu (1993).

In conclusion, numerical studies were performed to determine the force distribution on hump shapes of varying aspect ratios, representing the raised cell nucleus of a vascular endothelial cell. For a nonaxisymmetric semiellipsoidal hump, the least total force occurs when the major axis is aligned with the flow direction. Furthermore, for a fixed volume protruding above the cell membrane, there is a specific aspect ratio that gives a minimum total force on the cell nucleus. This is approximately the same as the average aspect ratio taken up by cell nuclei in vivo and we therefore postulate that the cells respond to flow in such a way as to minimize the total force experienced by the nuclei.

This work was supported by a studentship from the Wellcome trust for A.L.H. We are also grateful to Drs. Matthias Heil and Harvey Williams for several useful discussions on numerical techniques.

REFERENCES

Alkire, R. C., H. Deligianni, and J.-B. Ju. 1990. Effect of fluid flow on convective transport in small cavities. *J. Electrochem. Soc*. 137: 818–824.

Banerjee, P. K. 1994. The boundary element methods in engineering. McGraw-Hill, London.

Barbee, K. A., P. F. Davies, and R. Lal. 1994. Shear stress-induced reorganization of the surface topography of living endothelial cells imaged by atomic force microscopy. *Circ. Res.* 74:163–171.

Barbee, K. A., T. Mundel, R. Lal, and P. F. Davies. 1995. Subcellular distribution of shear stress at the surface of flow-aligned and nonaligned endothelial monolayers. *Am. J. Physiol.* 268:H1765–H1772.

Basmadjian, D. 1984. The hemodynamic forces acting on thrombi, from incipient attachment of single cells to maturity and embolization. *J. Biomechanics.* 17:287–298.

Brooks, S. B., and A. Tozeren. 1996. Flow past an array of cells that are adherent to the bottom plate of a flow channel. *Comput. Fluids.* 25: 741–757.

Caro, C. G., J. M. Fitz-Gerald, and R. C. Schroter. 1971. Atheroma and arterial wall shear: observation, correlation and proposal of a shear dependent mass transfer mechanism for atherogenesis. *Proc. Roy. Soc. Lond. B.* 177:109–159.

Chung, C., and B. G. Min. 1998. Fluid dynamic effects on endothelial cell morphology, *In* Abstracts of the Third World Congress of Biomechanics, Y. Matsuzaki, T. Nakamura, and E. Tanaka, editors. Hokkaido University, Sapporo, Japan. 170.

Damiano, E. R., B. R. Duling, K. Ley, and T. C. Skalak. 1996. Axisymmetric pressure-driven flow of rigid pellets through a cylindrical tube lined with a deformable porous layer. *J. Fluid Mech.* 314:163–189.

Davies, P. F. 1995. Flow-mediated endothelial mechanotransduction. *Phys. Rev.* 75:519–560.

Davies, P. F., T. Mundel, and K. A. Barbee. 1995. A mechanism for heterogeneous endothelial responses to flow *in vivo* and *in vitro*. *J. Biomech.* 28:1553–1560.

Davies, P. F., A. Remuzzi, E. J. Gordon, C. F. Dewey, Jr., and M. A. Gimbrone, Jr. 1986. Turbulent fluid shear stress induces vascular endothelial cell turnover *in vitro*. *Proc. Natl. Acad. Sci. USA.* 83:2114–2117.

Dewey, C. F. J., S. R. Bussolari, M. A. Gimbrone, Jr., and P. F. Davies. 1981. The dynamic response of vascular endothelial cells to fluid shear stress. *ASME J. Biomech. Eng.* 103:177–181.

Dimitrakopoulos, P., and J. J. L. Higdon. 1997. Displacement of fluid droplets from solid surfaces in low-Reynolds-number shear flows. *J. Fluid Mech.* 336:351–378.

Dussan, V. E. B. 1987. On the ability of drops to stick to the surfaces of solids. Part 3. The influences of the motion of the surrounding fluid on dislodging drops. *J. Fluid Mech.* 174:381–397.

Flaherty, J. T., J. E. Pierce, V. J. Ferrans, D. J. Patel, W. K. Tucker, and D. L. Fry. 1972. Endothelial nuclear patterns in the canine arterial tree with particular reference to hemodynamic events. *Circ. Res.* 30:23–33.

Fåhræus, R. 1929. The suspension stability of the blood. *Physiol. Rev.* 9:241–274.

Friedman, M. H., and D. L. Fry. 1993. Arterial permeability dynamics and vascular disease. *Atherosclerosis.* 104:189–194.

Fry, D. L. 1968. Acute vascular endothelial changes associated with increased blood velocity gradients. *Circ. Res.* 22:165–197.

Fung, Y. C., and S. Q. Liu. 1993. Elementary mechanics of the endothelium of blood vessels. *ASME J. Biomech. Eng.* 115:1–12.

Gaver, D. P., III, and S. M. Kute. 1998. A theoretical model study of the influence of fluid stresses on a cell adhering to a microchannel wall. *Biophys. J.* 75:721–733.

Henderson, J. M., D. L. Fry, and M. H. Friedman. 1994. Analysis of models of arterial permeability dynamics. *Biotechnik.* 17:717–725.

Herman, I. M., A. M. Brant, V. S. Warty, J. Bonaccorso, E. C. Klein, R. L. Kormos, and H. S. Borovetz. 1987. Hemodynamics and the vascular endothelial cytoskeleton. *J. Cell Biol.* 105:291–302.

Ingber, D. E. 1998. The architecture of life. *Sci. Am.* 278:48–57.

Ku, D. N., D. P. Giddens, C. K. Zarins, and S. Glagov. 1985. Pulsatile flow and atherosclerosis in the human carotid bifurcation: positive correlation between plaque location and low and oscillating shear stress. *Arteriosclerosis.* 5:293–302.

Lang, F., G. L. Busch, M. Ritter, H. Völkl, S. Waldegger, E. Gulbins, and D. Häussinger. 1998. Functional significance of cell volume regulatory mechanisms. *Physiol. Rev.* 78:247–306.

Levesque, M. J., and R. M. Nerem. 1985. The elongation and orientation of cultured endothelial cells in response to shear stress. *ASME J. Biomech. Eng.* 107:341–347.

Li, X., and C. Pozrikidis. 1996. Shear flow over a liquid drop adhering to a solid surface. *J. Fluid Mech.* 307:167–190.

Malek, A. M., and S. Izumo. 1996. Mechanism of endothelial cell shape change and cytoskeletal remodeling in response to fluid shear stress. *J. Cell Sci.* 109:713–726.

Olivier, L. A., and G. A. Truskey. 1993. A numerical analysis of forces exerted by laminar flow on spreading cells in a parallel plate flow chamber assay. *Biotech. Bioeng.* 42:963–973.

O'Neill, M. E. 1968. A sphere in contact with a plane wall in slow linear shear flow. *Chem. Eng. Sci.* 23:1293–1298.

Pedley, T. J. 1980. The Fluid Mechanics of Large Blood Vessels. Cambridge University Press, Cambridge, U.K.

Pozrikidis, C. 1992. Boundary Integral and Singularity Methods for Linearized Viscous Flow. Cambridge University Press, Cambridge, U.K.

Pozrikidis, C. 1997. Shear flow over a protuberance on a plane wall. *J. Eng. Math.* 31:29–42.

Price, T. C. 1985. Slow linear shear flow past a hemispherical bump in a plane wall. *Q. J. Mech. Appl. Math.* 38:93–104.

Ross, R. 1993. The pathogenesis of atherosclerosis: a perspective for the 1990s. *Nature.* 362:801–809.

Satcher, R. L., Jr., S. R. Bussolari, M. A. Gimbrone, Jr., and C. F. Dewey, Jr. 1992. The distribution of fluid forces on model arterial endothelium using computational fluid dynamics. *ASME J. Biomech. Eng.* 114: 309–316.

Shin, C. B., and D. J. Economou. 1991. Force and natural convection effects on the shape evolution of cavities during wet chemical etching. *J. Electrochem. Soc.* 138:527–538.

Wang, W., and K. H. Parker. 1995. The effect of deformable porous surface layers on the motion of a sphere in a narrow cylindrical tube. *J. Fluid Mech.* 283:287–305.

Weinbaum, S., G. Tzeghai, P. Ganatos, R. Pfeffer, and S. Chien. 1985. Effect of cell turnover and leaky junctions on arterial macromolecular transport. *Am. J. Physiol.* 248:H945–H960.

Yamaguchi, T., and Y. Yamamoto. 1995. Spontaneous alignment of a three-dimensional model of cultured endothelial cells under steady flow condition investigated using computational fluid mechanics, *In* Advances in Bioengineering, ASME-BED-Vol. 29, R. M. Hochmuth, N. A. Langrana, and M. S. Hefzy, editors. ASME, New York, 511–512.

Yamamoto, Y., and T. Yamaguchi. 1997. Natural shape and alignment of confluent endothelial cells minimizes the wall shear stress. *In* Advances in Bioengineering, ASME-BED-Vol. 35, K. B. Chandran, R. J. Vanderby, and M. S. Hefzy, editors. ASME, New York, 549–540.